

# Generative Model with Coordinate Metric Learning for Object Recognition Based on 3D Models

Yida Wang\* and Weihong Deng\*

\*School of Information and Communication Engineering, Beijing University of Posts and Telecommunications, Beijing, BJ 100876 China

**Abstract**—Given large amount of real photos for training, Convolutional neural network shows excellent performance on object recognition tasks. However, the process of collecting data is so tedious for human beings and the background of most photos are also limited which makes it hard to establish a perfect database because complex environments could not be easily accessed. In this paper, our generative model trained with synthetic images rendered from 3D models reduces the workload of data collection and limitation of conditions. From perspective of graph model, our structure is composed of two sub-networks: semantic foreground object reconstruction network based on Bayesian inference and classification network based on multi-triplet cost function for avoiding over-fitting problem on monotone surface and fully utilizing pose information by establishing sphere-like distribution of descriptors in each category which is helpful for recognition on regular photos according to poses, lighting condition, background and category information of rendered images. Firstly, our conjugate structure called generative model with metric learning utilizing additional foreground object channels generated from Bayesian rendering as the joint of two sub-networks. Multi-triplet cost function based on poses for object recognition are used for metric learning which makes it possible training a category classifier purely based on synthetic data. Secondly, we design a coordinate training strategy with the help of adaptive noises acting as corruption on input images to help both sub-networks benefit from each other and avoid inharmonious parameter tuning due to different convergence speed of two sub-networks. Such corruptions are applied automatically on two inputs of sub-networks which depend on variance ratio between output of the reconstruction sub-network and semantic segmentation masks, so it is both helpful to train a noise robust reconstruction network and an effective classification network. Our generative model with coordinate metric learning achieves the state of the art accuracy of over 50% on ShapeNet database with data migration obstacle from synthetic images to real photos. This pipeline makes it applicable to do recognition on real images only based on 3D models.

**Index Terms**—Bayesian rendering, triplet cost, synthetic image, semantic reconstruction, coordinate training, metric learning.

## I. INTRODUCTION

CONVOLUTIONAL neural networks such as AlexNet [1], Inception concept [2] and ResidualNet [3] work well on general image classification tasks by training on large amount of real training images with background and environmental variables such as ImageNet [4] and PASCAL [5]. Synthetic training data which could be generated in mass production [6], [7] also shows good performance on particular tasks such as distance and pose estimation [8], [9] since labels of camera

positions could be recorded accurately during data generation process in restricted condition. Triplet cost function [8] which is suitable for multi-task learning utilizes these accurate labels well, so the performance on model based learning is improved by making arrangements for triplet according to corresponding labels of synthetic data. As for exploiting geometric information related to pose estimation, recent works on object rotation and deformation combining CNN with auto-encoder [10], [11] solve tasks such as face rotation and intrinsic transformations for objects. Supervision information such as remote codes [10] gives a help on image transformation in regard to different purposes which makes auto-encoder more flexible for multi-task learning.

Though typical model based learning methods are effective in multi-task learning such as pose estimation [8] and category classification [12] with additional information which is captured by special equipment, they are not so applicable for training from synthetic images and testing on real photos with complex environments. Works on foreground object segmentation could be applied for weakening data migration problem from training on synthetic data and testing on real photos, but super pixel division method using SLIC [13] could not be expediently embedded into the classification pipeline.

In this paper, we propose a deep architecture combined with two sub-networks which are reconstruction network based on Bayesian render and classification network based on ZigzagNet trained only with synthetic data for category classification on real images. Like method in self-restraint reconstruction [14], our structure reconstructs foreground objects with specific surface colors related categories out of background learned from two types of synthetic training data rendered from models of ShapeNet [15] database, respectively one type with background images crawled from Flickr attached behind and another without background. Inspired by positive impact from depth images introduced in [8], [16] and method in [10], three additional channels from object reconstruction is concatenated to original RGB channels altogether as a six-channel data for classification sub-network training. Utilization of textured models from ShapeNet [15] avoids problem of over-fitting on monotone surface color lead by texture-less models in PASCAL 3D+ [17] which made it hard to learn a classifier directly based on descriptors. Our classifier is optimized using a jointed cost function composed of softmax loss and pose assisted triplet loss which is stable for data with large background differences and also effective for samples with tiny pose variance in triplet set. Gradients from jointed

cost function in the end for object classification is back-propagated to auto-encoder through concatenated structure to suit for reconstruction for particular objects acting as a supervision information like remote codes [10].

Initial attempts on FCN [18], [19], DeconvNet [20], VAE [21], [22] and SR [14] prove that pixel-wise regression methods are applicable for semantic reconstruction task using synthetic data. Based on Bayesian Theories [22], we modify CVAE [23], [24] both in encoder and decoder to make our structure a generative model with robust reconstruction result and able to generate semantic foreground objects without any other supervision information. The whole conjugate network aiming at reconstructing objects and classifying for categories in the same time is trained efficiently and effectively with adaptive noises for both inputs of two sub-networks. With the help of coupled noising ratios calculated by variances of generated images and ground truth masks, our training strategy avoids the problem of gradient vanishing from the final loss of classification network to the foremost reconstruction parametric model.

Experiment on PASCAL 3D+ [17] and subset of ImageNet [4] shows that our unified structure training on synthetic data could do object classification directly for real photos rather than using Nearest Neighbor classification in LDO [8]. Results show that accuracy is higher than AlexNet with the help of the automatic object construction. Utilization on pose information with our jointed cost function makes the classification accuracy much closer to the ones trained on real photos than some recent works like LDO [8] and SR [14].

In the following chapters, we describe how to effectively carry out recognition for real objects in photos based on 3D models with the help of semantic reconstruction of foreground objects and metric learning. We combine all functions into a concatenated deep neural network composed of two parts named with foreground object reconstruction sub-network and category classification sub-network. The unsupervised reconstruction network provides additional information including segmentation information, depth information and semantic information for supervised learning in the classification network for forward pass data. Classification sub-network with category labels also back-propagates gradients to the reconstruction network for effective parameter updating in training phase using coordinate metric learning. Suppose that we have paired synthetic training data of simulated images  $O$  and semantic depth masks  $M$ , reconstruction network with mapping function defined as  $map()$  and rendering function as  $ren()$ , classification network lead by multi-triplet cost function defined as  $cla()$  and paired adaptive corruption function as  $noi()$  and  $noi'()$ , the concatenated network is represented as  $cla(ren(map(noi(O))), noi'(O))$  in training and  $cla(ren(map(O)), O)$  in testing. Our network can be clearly understood through those separated functions defining different sub-networks. The generative model is embedded in the mapper  $map()$  and render  $ren()$  while metric learning is applied in the classifier  $cla()$ . At last, we make all those functions into a whole thing in perspective of effective parametric model training via corruption function  $noi()$ .

## II. TRAINING DATA PREPARATION

Representing information in the world using 2D rectangle images is easier than using 3D points cloud, so most visual information in the world are represented in form of photos likes those in ImageNet [4] database. We train deep neural network directly from images rendered from raw 3D models for the aim of testing on real photos. 3D models represented in relationship of points cloud together with textures could be projected to 2D space in view of camera using *VTK* toolkit, so we construct a new database which is consisted of two types of synthetic images rendered from 3D models of ShapeNet [15] database.

### A. Semantic Rendering

As shown in Fig. 1, our goal is to train a robust semantic rendering sub-network which provides additional information for classification sub-network with the aim similar to that of the self-restraint foreground object reconstruction network [14]. The reconstructed semantic segmentation result with depth information cascaded to the original RGB channels is used as input to the next classification network making the statistical gradient of the classifier able to be propagated to the reconstructed network. Reconstructed channels for foreground objects contain segmentation information, depth information and semantic color information which means that they can not only reflect more informative details about the foreground objects for analysis of the reconstruction network, but also help to train the classification network.

We render training images from 3D models in ShapeNet [15] database in paired form of .obj files describing geometry relationships of points clouds and .mtl files describing surface textures. Synthetic foreground objects are shot from positions on a sphere net combined with local triangles recursively subdivided from larger triangles which are initiated from a regular icosahedron [25] shown in Fig. 2(b). As range of view positions are limited in real world, we cut the whole sphere of points cloud along with two meridians which are vertical to  $z$  axis, so  $z$  coordinate  $V_z$  for ordinary objects are usually satisfy range of  $V_z \in [-0.1min(V_x), 0.6max(V_x)]$  where  $(V_x, V_y, V_z)$  is the coordinate of points cloud shown in Fig. 2(a). Shifting focal points are set within a range around the center of each object to simulate photos taken as close shots. As we want to utilize synthetic data to train a foreground semantic reconstruction network afterwards, background images are crawled from Flickr in which inappropriate images are shaken out afterwards to ensure that target objects are not included for a good representation on scene based images.

Inspired by the fast that depth image can provide complementary information for recognition on real images [8] by separating foreground target from background, we embed an semantic foreground object reconstruction sub-network in the whole generative model based on Bayesian coding. The output of the reconstruction network is concatenated to original images as a six channel data forwarded to the classification network. These concatenated channels reconstructed from simulated input images with background are expected to be similar to segmented object image with unique colors according to

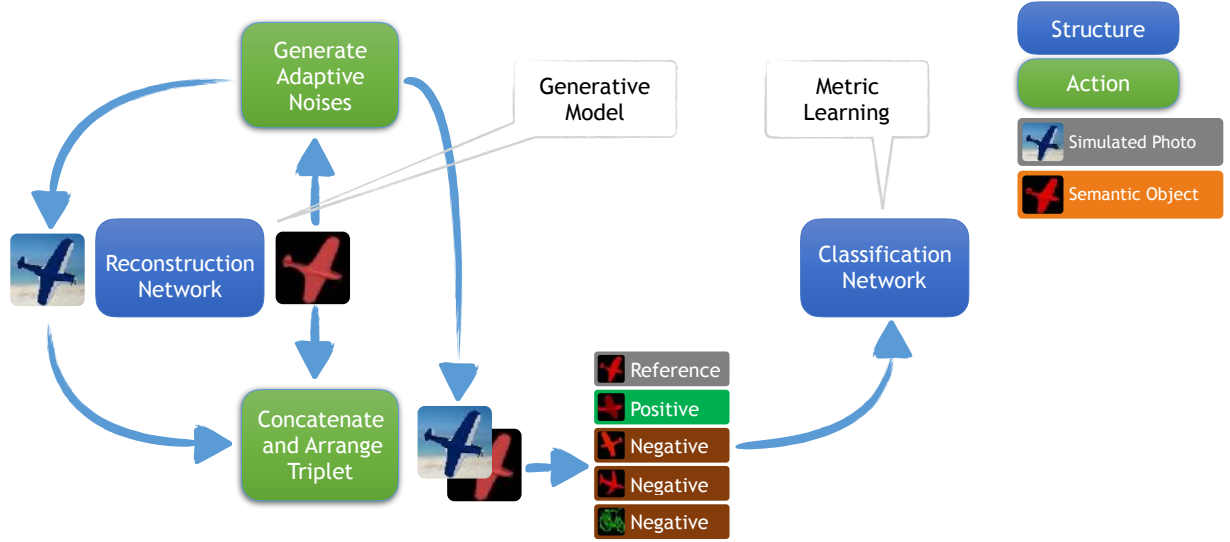


Fig. 1. Flowchart of generative model with coordinate metric learning using 3D models

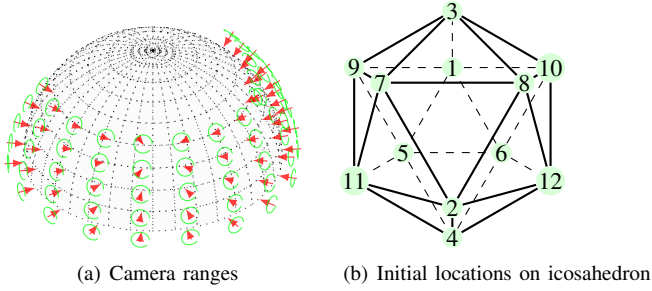


Fig. 2. Synthetic camera positions on the sphere with range of  $V_z \in [-0.1\min(V_x), 0.6\max(V_x)]$

category, so two types of images are rendered for the same camera parameters.

As shown in Fig. 3, we are facing a really challenging task with severe data transformation problem from synthetic data and real photos. There is not an end-to-end training anymore which is usually implemented in training directly from real photos. Two fatal issues can be tell from the mean images and normalized standard deviation images. Firstly, mean values and deviations visualized in rows of textured objects of ShapeNet and ImageNet in Fig. 3 show that gap between synthetic ones and real ones is still too large to train a recognition model directly from synthetic data. Secondly, shown like the mean values in row of semantic objects of ShapeNet, all foreground colors are set randomly with unique RGB values which is not evenly distinguishing between all categories.

### III. RECONSTRUCTION NETWORK

Reconstruction model is trained from paired synthetic images which are simulated images and semantic object segmentation masks. We apply two methods to make the reconstruction network more capable on semantic rendering for foreground objects. Firstly, we design a generative model using

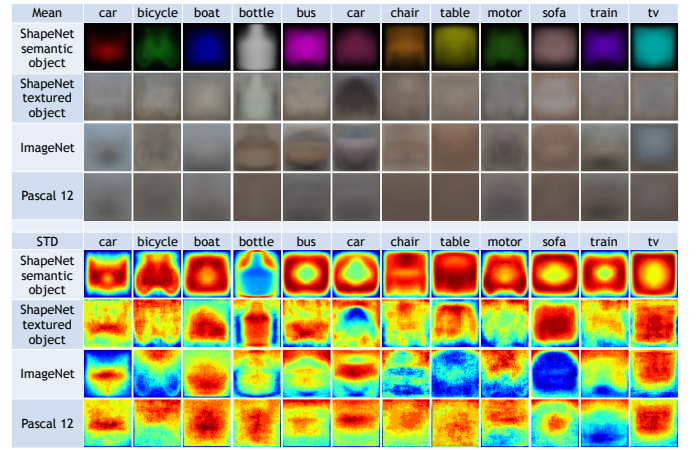


Fig. 3. Analysis on mean value and normalized heat map for standard derivation of images including two types of synthetic images and two types of real photos in large scale database

Bayesian inference based on VAE to make the decoder more capable on perceiving global information on objects compared to traditional pixel-wise convolutional rendering methods like FCN [18] and DeconvNet [20]. As goal of reconstruction is separating foreground object from background and rendering them with monotone color in regard to specific category, variational auto-encoder is modified to better utilize the latent space holding potential semantic information. Other supervision assistants for reconstruction like remote code described in face rotating [10] for multi-task learning according to the identities of objects are discarded while our gradients of jointed loss acting as supervision in classification sub-network is back propagated into the reconstruction network. Secondly, adaptive noises are applied automatically on foremost input feeding in reconstruction sub-network to fully exploit the back-propagated gradients of classification sub-network sequentially concatenated afterwards with multi-triplet loss, so our whole

structure is called generative model with coordinate metric learning. Both of the conjugate sub-networks are coupled with each others by utilizing the noising ratio.

#### A. Pixel-wise Generative Model

Our deep structure has the ability on preserving a manifold for object reconstruction with semantic surface rendering. As the expected output of this sub-network is representative in three aspects including depression on background, depth information retrieval and surface rendering with semantic color, the whole structure should be pertinent on specific categories of objects because the rendering mission is subjective rather than objective both in global and local patterns in RGB channels.

For such reconstruction mission, input sample  $X$  is mapped to output  $Y$  with the help of latent variables  $Z$  which acts as a transitional factor utilizing generative model. To keep the robustness and effectiveness on reconstruction mission of removing different backgrounds and rendering category based monotone colors, we design a generative model sharing some common features of VAE [21], [22] and CVAE [23], [24] which makes sure that a specific range of latent variables obeying Gaussian distribution can generate similar output  $Y$  according to specific input  $X$ . Main difference between our method and CVAE is that  $Y$  is served as generated target rather than additional condition for generating input  $X$ , so it's not necessary to feed  $Y$  into encoder and decoder. We define mapping function as  $map(X; \theta_1)$  and rendering functions as  $ren(z; \theta_2)$  for our coder with fixed  $\theta_1$  and  $\theta_2$ ,  $ren(z)$  is deterministic while  $z$  is randomly chosen.  $ren(z; \theta_2)$  is also a random variable in the space for reconstruction for input  $X$ . Inspired by the aim of variational auto-encoder which samples from latent space resulting to high probability results similar to the inputs, we set our expected target  $Y$  as result of objective rendering process with a joined mapper and render pair  $ren(map(X; \theta_1); \theta_2)$  which could be represented in form of probability as below:

$$p(Y) = \int p(Y|z; \theta_2)p(z)dz \quad (1)$$

Hence rendering output  $ren(z; \theta_2)$  is represented as a distribution  $p(Y|z; \theta_2)$  according to latent space  $z$ . For simplicity, Gaussian distribution use  $d$  in VAE is adopted in our model which means that  $p(Y|z; \theta_2)$  is represented as  $N(ren(z; \theta_2), \sigma^2 * I)$  with covariance defined by identity matrix  $I$  and scalar  $\sigma$ . Since  $p(Y|z)$  is an Gaussian, the negative log probability of  $Y$  is proportional to squared Euclidean distance between outputs  $ren(z)$  and targets  $Y$  which could be used in the final loss function. In regard to a pair of input and output, the main model  $p(Y)$  which maximizes the probability of the ground truth is the one based on the latent variable  $z \sim N(0, I)$ :

$$p(Y) = N(f(X), \sigma^2 * I) \quad (2)$$

where  $f$  is a deterministic function that we can learn from data which is a combination of mapping function  $m()$  and rendering function  $r()$ .

Cause we apply sampling strategy on the latent space  $z$ , there is a problem that probability  $p(Y|z)$  is almost zero for

most  $z$  and hardly contributes anything for the estimation of  $p(Y)$ . Our generative model attempts to sample  $z$  that are efficiently generating  $Y$  according to specific  $X$  and compute  $p(Y)$  based on those samples of  $z$ , so function  $q(z|X)$  is introduced which can utilize  $X$  and give us a distribution over  $z$  values that are likely to produce  $Y$ . Hopefully the space of  $z$  values that are likely under  $q$  is much smaller than the space of all possible sample in  $z$  space that are likely under the prior  $p(z)$ . Expectation of generated data given latent variable  $E_{z \sim q}p(Y|z)$  should be strongly on par with  $p(Y)$ , so we start with KL divergence between posterior probability  $p(z|Y)$  and distribution of encoder  $q(z|X)$ . Firstly, we apply Bayesian rule to  $P(z|Y)$ :

$$p(z|Y) = \frac{p(Y|z)p(z)}{p(Y)} \quad (3)$$

so we can represent our KL divergence like this:

$$D[q(z|X)||p(z|Y)] = E_{z \sim q}[\log q(z|X) - \log p(Y|z) - \log p(z) + \log p(Y)] \quad (4)$$

Here by applying Bayesian rule again on decoder  $p(Y|z)$  using posterior probability  $p(z|Y)$ :

$$p(Y|z) = \frac{p(z|Y)p(Y)}{p(z)} \quad (5)$$

In reference from the definition of evidence lower bound  $B$  for KL divergence  $D[q||p]$  described in [22], the evidence lower bound  $B$  for KL divergence  $D[q||p]$  could be represented as:

$$\begin{aligned} B(p, q) &= E_{z \sim q}[\log p(Y|z) + \log p(z) - \log q(z|X)] \\ &= \log p(Y) - D[q(z|X)||p(z|Y)] \end{aligned} \quad (6)$$

So we can rewrite the original KL divergence in Equation 4 as:

$$D[q(z|X)||p(z|Y)] = \log p(Y) - B(p, q) \quad (7)$$

By defining the evidence lower bound  $B$  which is an expectation related to  $z$ ,  $\log p(Y)$  is taken out as a standalone component from the expectation. Such representation not only makes it clear to define an optimization function for our sub-network in form of cost function in the end of the generative model, but also makes it possible for us to utilize noises to fully exploit the ability of reconstruction network. Because KL divergence  $D[q(z|X)||p(z|Y)] > 0$  which means that  $\log p(Y) > B(p, q)$  for any  $q(z)$ , variational inference tries to find the lower bound of the information of our training target  $\log p(Y)$  in form of its opposite number. We add random noises in input images  $X$  to make it more difficult to predict  $Y$  from  $X' = n_R(X)$ ,  $\log p(Y)$  turns smaller with noises and the evidence lower bound  $B$  is lower, too.

As  $q$  could be a flexible distribution, we can construct  $q$  depending on  $X$  and make  $D[q(z|X)||p(z|Y)]$  as small as possible. From perspective of Equation 7, we should maximize evidence lower bound  $B$  in regarding to  $\log p(Y)$ . Here we rewrite  $B$  as our optimizing target and define the cost function  $\mathcal{L}_r = -B$  of reconstruction network:

$$\mathcal{L}_r = D[q(z|X)||p(z|Y)] - \log p(Y) \quad (8)$$

The goal of cost function is maximizing  $\log p(Y)$  while simultaneously minimizing  $D[q(z|X)||p(z|Y)]$  which means that  $q(z|X)$  is optimized to match  $p(z|Y)$ . For definition of  $B$  in Equation 6 and Bayesian rule in Equation 5, we can get the final form of cost function for optimizing parametric model via stochastic gradient descend for encoder  $q(z|X)$  and decoder  $p(Y|z)$ :

$$\mathcal{L}_r = D[q(z|X)||p(z)] - E_{z \sim q}[\log p(Y|z)] \quad (9)$$

In perspective of feeding strategy of paired synthetic images and semantic foreground object reconstruction masks, our generative model takes advantage from both VAE and CVAE for our pixel-wise rendering task. Comparison on loss functions shown in Equation 10 shows that our model suits for foreground object reconstruction task better and easier. Our generative model can utilize a pair of data rather than just training auto-encoder from the same type of data with VAE [21], [22]. Meanwhile, Conditional VAE [23], [24] requires that conditional information  $Y$  should be used as jointed input with original information  $X$  rather than acting as rendering mask in the final output in our model. Supplementary information  $Y$  acts as supervision for auto-encoder in CVAE, we move  $Y$  directly to the end of the generative model based on decoder  $p(Y|z)$  to ensure that no additional labels are needed for testing which is intrinsic in foreground reconstruction process.

$$\mathcal{L}_{Ours} = D[q(z|X)||p(z)] - E_{z \sim q}[\log p(Y|z)] \quad (10)$$

$$\mathcal{L}_{VAE} = D[q(z|X)||p(z)] - E_{z \sim q}[\log p(X|z)] \quad (11)$$

$$\mathcal{L}_{CVAE} = D[q(z|Y, X)||p(z|Y)] - E_{z \sim q}[\log p(X|z, Y)] \quad (12)$$

### B. Parametric Model Optimization

Optimization process is similar to that used in VAE [21], encoder  $q(z|X)$  of our generative model is restricted in distribution  $N(z|\mu, \Sigma)$  where  $\mu(X; \theta)$  and diagonal matrix  $\Sigma(X; \theta)$  are arbitrary deterministic functions, so learnable parameters  $\theta$  should be optimized there. The remaining term  $D[q(z|X)||p(z)]$  is another KL divergence between two multivariate Gaussian distributions with the same latent dimensionality  $k$ . Because  $z$  is sampled from  $N(0, I)$ , divergence  $D[q(z|X)||p(z)]$  based on pair  $Y, X$  is shown below:

$$\begin{aligned} & D[N(\mu(p), \Sigma(p))||N(0, I)] \\ &= \frac{1}{2}(\text{tr}(\Sigma(p)) + (\mu(p))^T \mu(p) - k - \log \det(\Sigma(p))) \quad (13) \end{aligned}$$

As is standard in stochastic gradient descend, one sample of  $z$  for  $p(Y|z)$  could be an approximation of  $E_{z \sim q}[\log p(Y|z)]$ . So the full equation waiting to be optimized is:

$$\begin{aligned} & E_X[\log p(Y) - D[q(z|X)||p(z|Y)]] \\ &= E_X[E_{z \sim q}[\log p(Y|z)] - D[q(z|X)||p(z)]] \quad (14) \end{aligned}$$

If we take the gradient of this equation, the gradient symbol can be moved into the expectations. Therefore, we can sample values of  $z^{(l)}$  from the distribution  $q(z|X)$ , and compute the gradient of:

$$\mathcal{L}_r = \frac{1}{L} \sum_{l=1}^L \log p(Y, z^{(l)}) - D[q(z|X)||p(z)] \quad (15)$$

We can then average the gradient of this function over arbitrarily many samples of  $X$  and  $z$ , and the result converges to the gradient of Equation 14. However, a significant problem with Equation 14,  $E_{z \sim q}[\log p(Y|z)]$  depends not just on the parameters of  $p$ , but also on the parameters of  $q$ . We can also solve this problem by Equation 15 by re-parameterization trick [21]. Given  $\mu(X)$  and  $\Sigma(X)$ , the mean and covariance of  $q(z|X)$ , we can sample from  $N(\mu(X), \Sigma(X))$  by first sampling  $\epsilon \sim N(0, I)$ , then computing  $z = \mu(X) + \Sigma^{1/2}(X) * \epsilon$ . Thus, the equation we actually take the gradient of is:

$$\begin{aligned} & E_X[E_{\epsilon \sim N(0, I)}[\log p(Y|z = \mu(p) + \Sigma^{1/2}(p) * \epsilon)] - \\ & D[q(z|X)||p(z)]] \quad (16) \end{aligned}$$

## IV. RECONSTRUCTION WITH METRIC LEARNING

Direct reconstruction network using RGB channels without dependency on the number of categories makes it easy to apply on different databases. As reconstructed channels are expected to be similar to subjective semantic masks, pixel-wise softmax loss is not necessary to be applied for our rendering pipeline. Meanwhile, Euclidean distance might lead to a severe problem caused by specific three dimensional pixel vectors for different categories of foreground objects. Assuming that a descriptor of the reconstructed channels from one sample is represented as  $r = [\text{pixels}_r, \text{pixels}_g, \text{pixels}_b]$  where  $\text{pixels}$  are feature for a single channel, the effectiveness of back-propagated Euclidean loss directly depends on the assigned absolute RGB values of masks which means that greater disparity between two classes matters more than the minor one. This is a disaster when there are so many categories that we can't attribute effective RGB colors anymore for a discriminative rendering.

We increase the mutual information between features of our training data and real photos by exploiting discriminant factors to minimize over-fitting problem triggered by absence of textures. Based on additional information apart from category, ZigzagNet is pre-trained using a multi-triplet cost function joint with an optional pair wise term for speeding up convergence based on labels of poses and lighting conditions. Then additional data with different focal points is used for fine-tuning with softmax loss to imitate more real scenes. Our training method is introduced for the aim of extracting descriptors for classification using NN classifier without other feature transformation such as softmax and SVM classifier which doesn't suit for data migration between synthetic data and real images. We evaluate the performance of our work on output of the penultimate layer of the net before the last inner product matrix. Our discriminant descriptor satisfies NN classifier better than models trained from real images and is even similar to the performance of AlexNet [1] descriptors which is also trained from realistic data using larger parametric model.

### A. Compact Classification Network Structure

As our conjugating generative model for reconstruction is so compact which is just 14 MB in disk, we apply concept of ZigzagNet which is just 6.2 MB as replacement of 240 MB AlexNet as classification sub-network. So the overall model

size of our conjugating model is just about 20.2 MB in disk which is much smaller than most popular recognition deep models like AlexNet and Inception models. Another reason for applying Zigzag module in replace of AlexNet is that such compact model is less likely to have over-fitting problem from synthetic data and real photos.

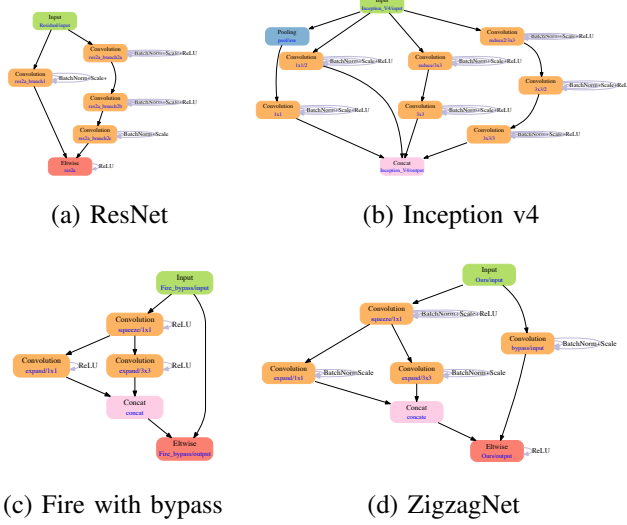


Fig. 4. Core micro structures composed of several layers in ResidualNet [3], Inception v4 [26], SqueezeNet [27], SqueezeNet with bypass and our ZigzagNet.

Data migration problem from synthetic training data and real testing data could not be completely eliminated, we do learnable channel-wise compression between micro architectures for deep structure to avoid over-fitting while keeping the depth and width of network to remain the ability of learning discriminant features from training data together with cost function. SqueezeNet [27] defines CNN micro architecture as individual layers while macro architecture as the big-picture organization of multiple modules with some shared features. Our ZigzagNet has tinier parametric model compared to AlexNet and better performance compared to SqueezeNet [27] with the same macro architecture where sequence and output dimension of every micro architectures are all the same. ZigzagNet combines SqueezeNet with residual concept [3] and gets rid of fully connected layers with Zigzag module instead of FCN architecture [18]. It is concatenated of repetitive micro Zigzag modules composed of three  $1 \times 1$  and one  $3 \times 3$  convolutional layers in a zigzag style of 3 steps: channel wise squeezing for principal representation, reception fields expanding by parallel connection of multi-scale convolution kernels and consolidation by adding  $1 \times 1$  convolutional layer to bypass the original information before squeezing to keep the learning process stable while remaining the size of parametric model. Input to a single module is compressed by a  $1 \times 1$  convolutional layer which does linear transformation like PCA [28] on 1D channel vectors within 3D input cubics to make the following parameter model compact and representative. Output in a single module within macro architecture is joined with bypassed original information by a convolutional layer as the input of next module to keep the learning process

stable. Based on a single Fire module of bypassed SqueezeNet shown in Fig. IV-A, ReLU operation on the expand layer before the element wise sum layer is moved to the output of Fire module to eliminate the scale difference between two inputs of the element wise operation layer and make information from both branches compressed at the same time. For convenience of comparison experiments, depth of macro structure of ZigzagNet is set as the same as AlexNet and SqueezeNet in account of micro structures with channel-wise representation.

### B. Multi-triplet Based Pre-training

We take advantage of our training data generated from two camera modes separately using multi-triplet cost and softmax cost. As background images are added for keeping environmental deviation related to real photos, training with category labels based on texture-less models leads to over-fitting on distinguishing edges of objects against background so that objects without clear boundary against background in real images won't be recognized well. We introduce a special triplet cost to utilize information contained in labels of poses, lighting conditions of items.



Fig. 5. Triplet set with 5 samples where reference and positive samples are fixed and 3 negative samples (1 pose negative + 2 class negative) are used for multi task learning on camera pose related descriptor distribution and classification.

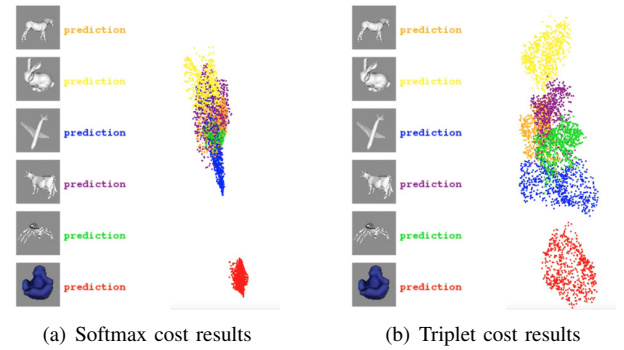


Fig. 6. 3D feature visualization with PCA matrix calculated from descriptors of our jointed loss.

Our multi-triplet cost function which is modified from work of [8] together with an optional pair wise term is used in the initiation process to enhance the ability for recognizing physical structure characteristics of particular objects both about themselves and towards others. Fig. 6 shows that pose related triplet training has a sphere-like distribution of descriptors from 3D models and 4 Nearest Neighbor Prediction indicates that trained parametric model has ability on both identification on object categories and distribution regression on object



poses. Sub-figure(a) in Fig. 6 shows that learning in early stage over fits the blue surface of Ape which is bad for both classification and feature distribution. Our multi-triplet loss solves this problem on surface texture at last which is not only capable for a multi task learning on poses, but also beneficial for prediction on categories. Triplet makes it possible to train a model guided with substantial labels including object poses, lighting conditions and camera modes which are accurately recorded with training sample to fully exploit the information in objects themselves rather than raw information given by just huge amount of background in real images. As triplet cost doesn't use label as an supervision, we arrange samples in proper sequence for the model construction process. A particular loss set is composed of a reference sample, a positive sample and several negative samples:

$$\mathcal{L}_{tri-set} = \mathcal{L}_{pair}(x_i, x_j) + \sum_{(x_i, x_j, x_k) \in \mathcal{T}} \mathcal{L}_{tri}(x_i, x_j, x_k) \quad (17)$$

where  $\mathcal{L}_{pair}(x_i, x_j) = \|f(x_i) - f(x_j)\|_2^2$ . As shown in Fig. 5, our triplet set is composed of 5 samples, the positive sample is selected as the one with close pose from reference sample or only has a different lighting condition which is the same pose and 3 negative samples are selected as one differs more in pose from the same class and two from other classes or sub-classes. Inspired of [8], the problem of gradient vanish in traditional triplet [29] is solved. Correspondingly, large variance in background images from Flickr makes the gradient easy to explode because every channel varies much, so we further apply natural logarithms on loss of a triplet. Feature distance in triplet loss is modified from Euclidean distance to its square form where distribution of learned descriptors has a manifold of sphere as shown in Fig. 6(b) which is related to camera positions on a sphere rather than a manifold of cubic in low dimensional spaces. This also makes the learning process more stable for samples which differs little, so tiny difference between reference and positive sample without background which are close will not lead to a NaN gradient which might appear in use of Euclidean distance in [8].

$$\mathcal{L}_{tri} = \ln(\max(1, 2 - \frac{\|f(x_i) - f(x_k)\|_2^2}{\|f(x_i) - f(x_j)\|_2^2 + m})) \quad (18)$$

where  $f(x)$  is the input of the loss layer for sample  $x$  and  $m$  is the margin for triplet. Denote that  $D_{ij} = \|f(x_i) - f(x_j)\|_2^2$  and  $D_{ik} = \|f(x_i) - f(x_k)\|_2^2$ , so the partial differential equations for the input of triplet loss layer are:

$$\begin{aligned} \frac{\partial \mathcal{L}_{tri}}{\partial f(x_i)} &= \frac{D_{ik}(f(x_i) - f(x_j)) - (D_{ij} + m)(f(x_i) - f(x_k))}{\mathcal{L}_{tri}(D_{ij} + m)^2} \\ \frac{\partial \mathcal{L}_{tri}}{\partial f(x_j)} &= \frac{D_{ik}(f(x_j) - f(x_i))}{\mathcal{L}_{tri}(D_{ij} + m)^2} \\ \frac{\partial \mathcal{L}_{tri}}{\partial f(x_k)} &= \frac{f(x_i) - f(x_k)}{\mathcal{L}_{tri}(D_{ij} + m)} \end{aligned} \quad (19)$$

For convenience on training data preparation process, we set the positive and the reference sample fixed in a triplet set and use them straightly as the pair wise term if it's needed. As triplet based training is much more slower in convergence, we train with samples without background at first and attach the

pair wise term in a triplet set to make it converge quicker. The pair wise term is only used to make the descriptor robust to small variance in different lighting conditions rather than much more complex backgrounds, we remove it later in the background added training stage. We directly apply NN classifier to maintain the ability of distinguish different classes apart and have a manifold distribution on features to capture the geometry of corresponding poses at the same time. Positive and negative samples in  $(s_i, s_j, s_k)$  are carefully selected regard to the reference samples. Positive sample in a set is always selected as one in the same class with reference samples with a similar pose. The key point is that positive samples should either have a slight different viewing angle from camera compared to the reference samples or have a different lighting condition.

### C. Fine-tuning with Additional Data

Triplet training based on poses has a restriction of fixed focal points. We add softmax loss for fine-tuning based on close shot images with shifted focal points which are moved from the center of object to the head of objects regards to the shift angle from the axis of front view. Shift distance of focal points varies directly as the distance from the view position to horizontal axis of the object which could be represent as  $(F'_x, F'_y, F'_z) = (F_x, F_y, F_z) + 0.2((C_x, C_y, C_z) - P_{axis})$  where  $F$  represents the focal points used for the camera shots,  $C$  represents the camera position on the sphere and  $P_{axis}$  represents the intersection point of the axis of front view and the surface of the regular view sphere. Distribution of descriptors projected with 3 dimensional PCA matrix shows that special samples from real test images could be better clustered with other normal samples in the same class after fine-tuning and all samples are set apart better according to categories. Additional rendered data gives a help on reducing intra-class variability while keeping the geometry relationship of regular samples based on pre-trained model.

## V. COORDINATE TRAINING FOR CONJUGATE STRUCTURE

Our network concatenated by reconstruction and classification sub-network is also correlated on two inputs of both sub-networks which makes them relatively coordinate in training stage in form of higher convergence speed and classification accuracy. Our coordinate training concept based on coupled noising ratio  $P_N$  and  $P_C$  overcomes the difficulty of fully utilizing each other's forward outputs and back propagated gradients. The following part describes how we use coupled ratios on each input of sub-networks to make the training process more efficient than training them with the same original information all the time.

### A. Adaptive Noise Assistant for Information Feeding

Here the effectiveness of multiple sub-networks is raised by applying adaptive noises for different input data. Two sub-networks should not be simply concatenated together even if we want to utilize loss functions of both of them because there are problem of unbalancing in the whole network if we just

concatenate the output of reconstruction network to synthetic simulated image channels accordingly. As shown in Fig. 8, the reconstruction network is only able to generate average images of all semantic depth masks with foreground objects from those simulated images in the beginning, so those three concatenated channels are not discriminant at all for the classification network. Given the assumption that our training data is evenly distributed in batches for different categories, The classification results and parametric model from our pipeline will be both similar to the one without reconstruction network trained because the statistically back propagated gradients are not effectively passed to the reconstructed channels. This means that the two parts of the whole network not so relevant to each other and also won't take benefits from each other's forward outputs and back propagated gradients.

If original synthetic images are represented as object channels  $O$  and semantic depth masks are represented as masks  $M$ , reconstruction network with input  $Input_R = [O]$  produces reconstruction channels  $M'$ . The data fed in classification network is represented as a channel-wise concatenated tensor as  $Input_C = [O, M']$ . Direct training for the classification network based on  $[O, M']$  will lead to a severe problem of over-fitting on reconstructed channels because the variance of  $M'$  is far smaller compared to the other three original channels which means that the classification network utilizes few things from reconstructed channels, so the classification result also differs not so much without  $M'$ :  $cla(Input_C) \approx cla(Input_R)$ . For perspective of statistical gradient decent for the reconstruction sub-network, gradients passing back through  $Input_C$  will not be effective also due to the absence of correlation between the classification loss and information in  $Input_C$ . We propose an efficient strategy using adaptive noise on the simulated data separately on the input of reconstruction network and classification network to solve this problem.

We utilize coupled noising function  $n_R$  and corruption function  $n_C$  for restricting information feeding in the original simulated images separately which are defined as:

$$\begin{aligned} n_R(input) &= P_N \text{ Ran} + (1 - P_N) \text{ input} \\ n_C(input) &= P_C \text{ Ran} + (1 - P_C) \text{ input} \end{aligned} \quad (20)$$

where  $P_N$  is noising ratio for synthetic input data fed in reconstruction sub-network,  $P_C$  is corruption ratio for classification sub-network and  $\text{Ran}$  is random noises with the same shape of  $input$  from a uniform distribution in the range  $[\min(input), \max(input)]$ . Here we ensure that information from the simulated synthetic images are partially used according to the variation of the reconstructed samples and semantic masks. We set noising ratio  $P_N$  as hyperbolic tangent function applied on ratio of variance between reconstructed images and semantic masks in current batch in training stage while the corruption ratio  $P_C$  as output of hyperbolic tangent function applied on the result of  $1 - \gamma(\alpha, \beta)P_N$ , so we can see that  $P_N$  and  $P_C$  are strongly correlated with each other through  $\gamma(\alpha, \beta)$ . Assuming that hyper parameters  $\alpha$  and  $\beta$  are set to be the same,  $\gamma$  will be 1 which means that we can easily represent  $P_C$  using  $P_N$ . Both ratios could be represented in Equation

21.

$$\begin{aligned} P_N &= \tanh(\alpha \frac{Var(M')}{Var(M) + mar}) \\ P_C &= \tanh(1 - \tanh(\beta \frac{Var(M')}{Var(M) + mar})) \end{aligned} \quad (21)$$

Here we usually set hyper parameters  $(\alpha, \beta)$  as 0.25 and 2 according to results of experimental tests. For general speaking, the noising ratio and corruption ratio are coupled as Equation 22.

$$P_C = \tanh(1 - \tanh(\frac{\beta}{\alpha} \arctanh(P_N))) \quad (22)$$

This means that the classification network plays different roles in the whole training process which can be roughly divided into two unique stages. Such strategy on training procedure ensures that information in simulated synthetic images is well utilized because the classification network could try best to learn from reconstructed channels in absence of effective information in image channels, meanwhile the orderly concatenated sub-networks and spatially concatenated six-channel input data which is the junction between two sub-networks are trained in balance with effective gradients. Our training strategy makes the whole network easier to get converged than generative adversarial networks [30], [31] where the generator and discriminator are sometimes trained separately according to the loss or discriminative accuracy. Similarly, parametric model in our network benefits from each others when foreground object reconstructor and classifier are always supervising each others in the training stage. If we regard them as generator and discriminator like concept in GAN, the parametric model are updated with difference paces which means that it's always updating parametric model even with zero gradients defined by the variance of generated channels.

## VI. EXPERIMENTS

### A. Experiments on ShapeNet Database

1) *Visualization of Reconstruction*: Basic experiments use purely synthetic images rendered from 3D models for both training and testing data with little data migration problem to prove that our generative model has a strong fitting capability. Reconstruction results of synthetic training images rendered from ShapeNet database show that our structure has the ability to reconstruct ideal pixel-wise semantic foreground objects with discriminant colors. Twelve unique RGB color set representing for different classes are used as semantic segmentation masks for training shown in Fig. 7(b) which means that the reconstructed channels are represented by RGB values for visualization rather than channel-wise one hot coding used in AAE [32] with unfixed number of channels. There are two main advantages contributed by direct reconstruction compared to the widely used one-hot coding [33] by expanding channels. Firstly, reconstructed RGB channels could be widely used for representing segmentation masks in real database because it could be easily visualized for the users. Then large amount of channels make the pixel-wise representation too sparse and to be stored efficiently on disks



while the space of a single sample of our reconstructed RGB image is almost fixed even if the number of object categories is huge. We use Euclidean distance cost function instead of softmax cost function for decoder without dependency on uniform distribution on three channels which means that semantic masks in two different categories with similar color sets are not less discriminative compared to ones in another pair of colors with bigger Euclidean distance. Our deep structure is more discriminant and robust from perspective of the reconstruction result, reconstruction target in form of semantic depth information in Fig. 7(b) could be retrieved well in Fig. 7(d) while suppressing the background at the same time. Similar network structure without variational variables is simply represented as fully convolutional network [18] in Fig. 10(e), it shows that contours are not reconstructed as clear as our generative method and the colors in single object also differ more which means that there are not enough meaningful semantic information according to the categories of foreground objects.

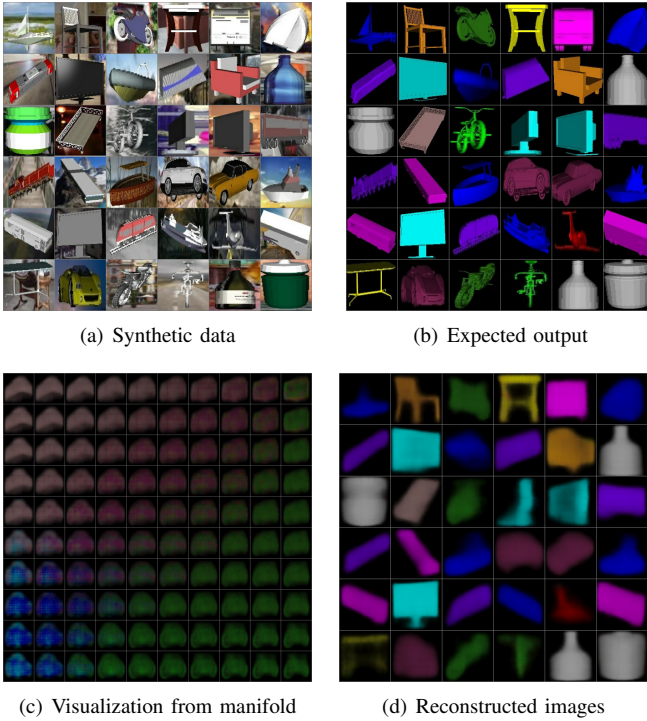


Fig. 7. Experiments on synthetic training data from ShapeNet models

As for the training process, reconstruction procedure shown in Fig. 8 satisfies for our expectation on utilization of variational latent space well. The reconstruction network in initial training stage is only able to reveal average color of all masks together with convex hull of objects by suppressing surrounding background. Then the outputs of the reconstruction network according to input samples in categories with less intraclass variance such as bottles are reconstructed clearer. Finally, pixel-wise reconstruction for samples from complex categories like planes and bikes with larger intraclass variance are also extracted successfully from background together with depth information in form of different local brightness on surface of objects.

In perspective of cost functions, the visualization of reconstructed channels in Fig. 8 explains how our generative cost function for reconstruction network works. Loss of decoder based on Euclidean distance in the first stage of training matters more than KL divergence component for encoder which behaves similarly to principle component analysis [34], [35] using singular value decomposition to ensure reconstruction error as small as possible, so the average color and contour of samples are reconstructed quickly in this initial stage. This explains why samples in categories with little intraclass variance is reconstructed better in this stage. Then loss component defined by KL divergence takes effect for rendering details to make sure that input samples from different categories with larger intraclass and smaller interclass variance are learned better according to reasonable latent space. Two components of the reconstruction loss play their own roles at different stages of training which means that Euclidean distance component make the decoder quickly fit the mean value of the training data and the intraclass variance of simple samples, then KL divergence component makes a finer fitting for interclass variance of samples while keeping previous samples reconstructed stably by utilizing latent space well with encoder.

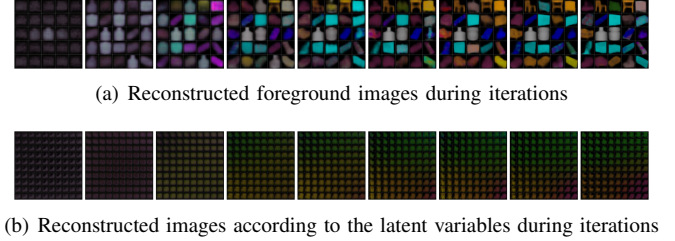


Fig. 8. Visualization of reconstructed samples according to inputs and randomly selected latent variables

2) *Parameter Analysis in Training:* Although we only concatenate the output of the previous sub-network to the later one in graph model for two unique networks, this conjugate network works as a whole part in the training stage rather than gets trained separately. As shown in Fig. 9(a), both KL divergence loss and the Euclidean loss in the reconstruction network are optimized in similar trends and converge in similar training stage. If we compare them in details of optimization paces, it's obvious that there is a rapid drop of the KL divergence loss in Fig. 9(i) at the very beginning of training. Then the loss keeps the same in a particular range for a long time while the Euclidean loss keeping going smaller in Fig. 9(j) because the encoder helps to construct a reasonable mapping space containing clusters of coders of inputs which is not necessary to be largely fine-tuned like the renderer. Corruption ratio plays an important role for training concatenated network, analysis on relationship of losses and corruption ratio explains how adaptive noises are applied and take effects. Envelope of variation ratio between reconstructed images and mask images in Fig. 9(d) monotonically increase which means that discriminant information in reconstructed images increases gradually. Two corruption ratios shown in Fig. 9(e) and Fig. 9(f) defined for inputs feeding in reconstruction network and classification

network are in negative and positive correlation separately with the variation ratio in Fig. 9(d) which means that difficulty on training of reconstruction network increases and the one for classification network decreases during training. Coupled corruption ratios make the reconstruction sub-network utilize back-propagated gradient of classification sub-network more efficiently and the classification sub-network utilizes all six input channels evenly without over-fitting on synthetic RGB channels compared to reconstructed channels at the beginning due to the fact that reconstructed ones are almost the same. By reducing information of input images for classification sub-network, information in all six channels are always balanced during training. Gradient from all six channels in classification network could be fully utilized in the beginning rather than only from three of them in synthetic images with background. It's more interesting to have a look on the intersection of three lines in Fig. 9(b) when two corruption ratios applied on reconstruction and classification networks equals to each other, here it shows that loss of classification in Fig. 9(g) is already decreased substantially and converges in a much smoother way in training afterwards without unstable loss turbulence. This means that synthetic RGB images with background are not over-fitted before there are enough discriminant information in the reconstructed channels which is reflected from the variance ratio in Fig. 9(d), so the corruption ratio of simulated images for classification network is smaller than corruption ratio for reconstruction network from now on and keeps going down to feed more information to classification network as the reconstructed channels are more and more discriminant.

3) *Advantages to Other Pixel-wise Reconstruction Methods:* As reconstruction sub-network of our conjugate structure depends on VAE, the final reconstruction result is similar to the one learned from CVAE [23], [24]. The advantage of our structure compared to conditional generative model alone is shown in the learning process between Fig. 10(a) and Fig. 10(c) where conjugate network learns more faster than conditional generative model due to the contribution of the classification sub-network through back-propagated gradients from supervision of object categories and adaptive noises. Our conjugate generative model also performs better than other popular pixel-wise regression models such as fully convolutional network [18], [19] and DeconvNet [20]. As shown in Fig. 10, our GM-ML has advantages both on speed of learning and precision of reconstruction results. Results of methods like DeconvNet with FCN as first few layers shows that directly doing a pixel-wise coding from simulated images to semantic masks does not work as well as ours because traditional FCN and DeconvNet treat semantic segmentation tasks in a pixel-wise softmax prediction way in the training process without hidden probabilistic variables, direct learning from input makes it less robust to noises for FCN. Firstly, initial FCN reconstruction shown in Fig. 10(e) easily lead to an over fitting problem for synthetic data where the average colors and contours are learned at first which is not so reasonable for differences between categories. Secondly, final result of FCN in Fig. 10(e) also have problem of rendering monotone RGB colors according to unique categories where a single object has more than one colors on the surface. An

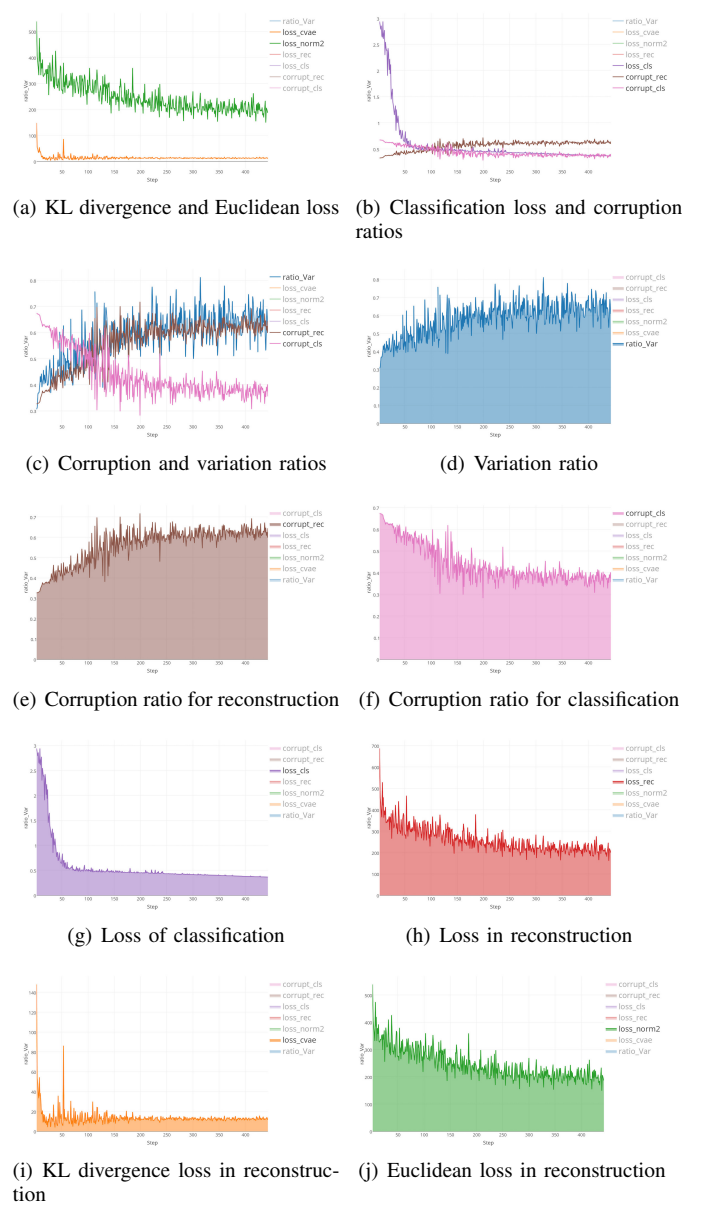


Fig. 9. Line charts of training parameters for experiments based on ShapeNet.

advantage of our GM-ML is making it possible to train a pixel-wise coding strategy from regression procedure which is more similar to unsupervised training with hidden meaning of category clusters in the latent space, it can also be regarded as a supervised method because of the utilization of paired input and desired reconstructed output as semantic masks. Our method shown in Fig. 10(a) shows that it fits for the learning target shown in Fig. 7(b) well. If corruption noises are fixed rather than adaptively changed according to output of reconstruction channels like result in Fig. 10(b), the learning progress is much slower.

4) *Visualized Feature Distributions:* We visualize the distribution of features in the end by projecting extracted features of classification sub-network to two dimensions using principal component analysis [28] and independent component analysis. Reconstructed results in Fig. 11 shows that our conjugate gen-

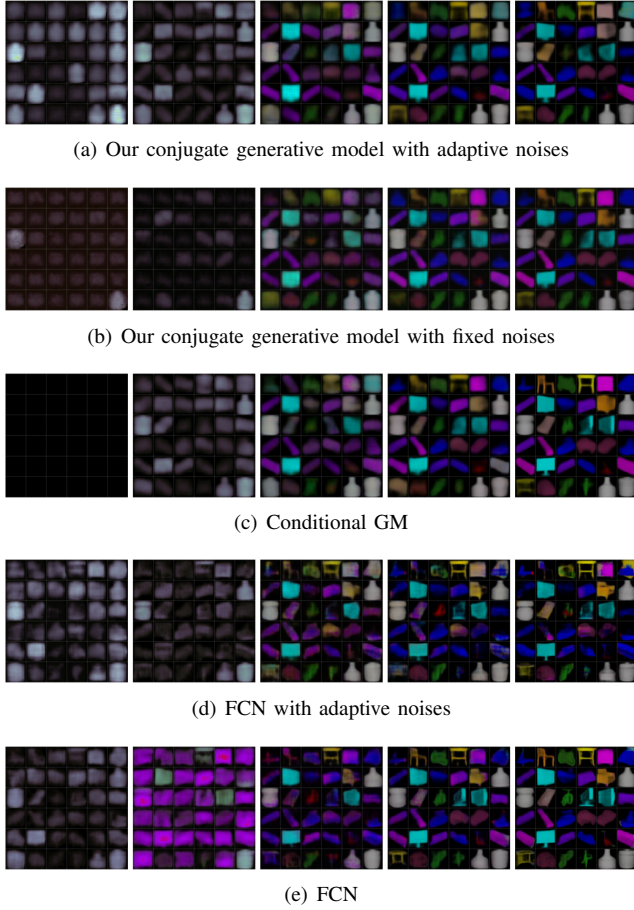


Fig. 10. Visualization of reconstructed samples according to inputs and randomly selected latent variables

erative model with adaptive noises for training has advantages both in the accuracy of reconstruction and desired distribution of the final features. PCA projected features in Fig. 11(a) can not separate features among categories as good as ours in Fig. 11(c). This comparison experiment shows that directly concatenating a classification network to conditional generative model without back-propagating gradients from classification network could not utilize the reconstructed channels well due to the absence of categories information. Reconstructed foreground objects using FCN [18] concatenated with a classification network shown in Fig. 11(b) have more blended colors than ours with monotone colors in Fig. 11(c) which means that the pixel-wise reconstruction task can not obtain stable rendering ability according to categories without using generative model even when it can also reconstruct contours well.

Table.I shows results of testing on synthetic images rendered from ShapeNet [15] with backgrounds and training with another synthetic database rendered with different backgrounds and object poses. Our conjugate deep structure with the help of the foreground reconstruction sub-network is also more capable for classification tasks than other popular deep structures. Table.I shows that our generative model(GM-ML\_1) of which output of the reconstruction sub-network is concatenated as a part of the input of ZigzagNet for classification

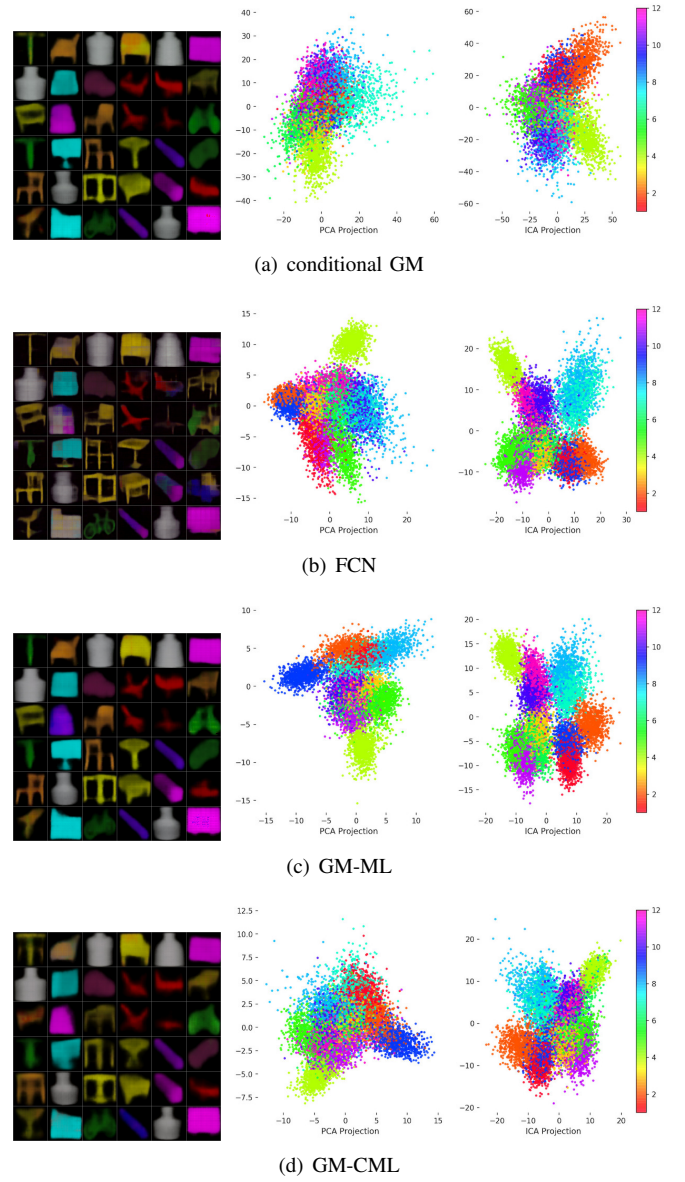


Fig. 11. Reconstruction samples of synthetic images rendered from 3D models of ShapeNet for recognition and low dimensional projection using PCA and ICA. GM-CML means that the conjugate generative model is trained with adaptive noises.

achieves the accuracy of 97.9% which is 7.8% higher than the one trained from ZigzagNet. This big improvement shows that the additional channels of semantic foreground object extraction is also helpful for the classification network as long as difference between training and testing data is not so much. Comparison experiments on different reconstruction sub-networks show that generative model retrieves the hidden category information in form of visualized colors well enough with 5.1% improvement on classification accuracy compared to FCN.

### B. Experiments on ImageNet Database

Real photos of PASCAL and ImageNet for test is collected from PASCAL 3D+ [17] database which enriches PASCAL VOC 2012 with 3D models together with original real images



TABLE I

CLASSIFICATION ON RENDERED SAMPLES FROM SHAPENET DATABASE. TRAINING DATA INCLUDES REAL PHOTOS, MODELS FROM PASCAL 3D+(PASMODEL) AND MODELS FROM SHAPENET(SHAMODEL). GM-CML<sub>1</sub> MEANS THAT OUR CONJUGATE GENERATIVE MODEL IS TRAINED WITH ADAPTIVE NOISES AND THE OUTPUT OF RECONSTRUCTION NETWORK IS CONCATENATED WITH THE INPUT OF ZIGZAGNET. GM-ML<sub>2</sub> MEANS THAT THE CLASSIFICATION NETWORK IS ALEXNET.

Method	Result	Accuracy	Model size
GM-CML <sub>1</sub>		96.3%	20.2 MB
GM-ML <sub>1</sub>		97.9%	20.2 MB
GM-ML <sub>2</sub>		97.1%	20.2 MB
FCN [18]		91.2%	20.2 MB
DeconvNet [20]		92.7%	20.2 MB
AlexNet [1]		86.2%	240 MB
SqueezeNet [36]		84.7%	4.8 MB
ZigzagNet [37]		90.1%	6.2 MB

in ImageNet and PASCAL. We do classification using outputs from softmax classifier which is the last layer in classification network to evaluate the performance. We render training data from models of PASCAL 3D+ and ShapeNet database with the same tools used in SR [14] and ZigzagNet with random background and poses, so some experiment results are collected from original papers if our testing results are similar to previously declared ones. Experiment in Table.II on trained network for regular photos from ImageNet attached in PASCAL 3D+ [4] shows that conjugating generative model with the help of adaptive noises could extract semantic foreground object information from background better compared to other popular and recent networks, achieving the state of the art accuracy of 50.5% in real photos from ImageNet. Comparison experiments on other reconstruction methods such as fully convolution network [18] and deconvolution network [20] show that latent variables in our generative model is helpful on extracting category informations in the foreground semantic masks which contribute to about 10% accuracy rising. We use the same reconstruction network parameter and macro structure for our conjugate generative model, FCN and DeconvNet, the difference in the reconstruction sub-network is that FCN is lack of the latent variables in the middle layer and un-pooling layer in DeconvNet is operated by the indexes of max elements according to the previous pooling layers. Visualization of the reconstructed channel in Fig. 12(d) shows that it has advantage in details of objects to segmentation results without texture information and also have ability on suppressing close-up background compared to depth images. Object reconstruction is applicable in extracting objects in real images which not only reflects contrast between object and background, but also suppress highlights in background. Although foreground objects reconstructed through single channel depth images could give a help on doing classification on real photos by means of concatenating reconstructed channel to RGB channels, there is still a gap between SR [14] and our method based on three channel object reconstruction with semantic colors.

Our compact generative model based on ZigzagNet could

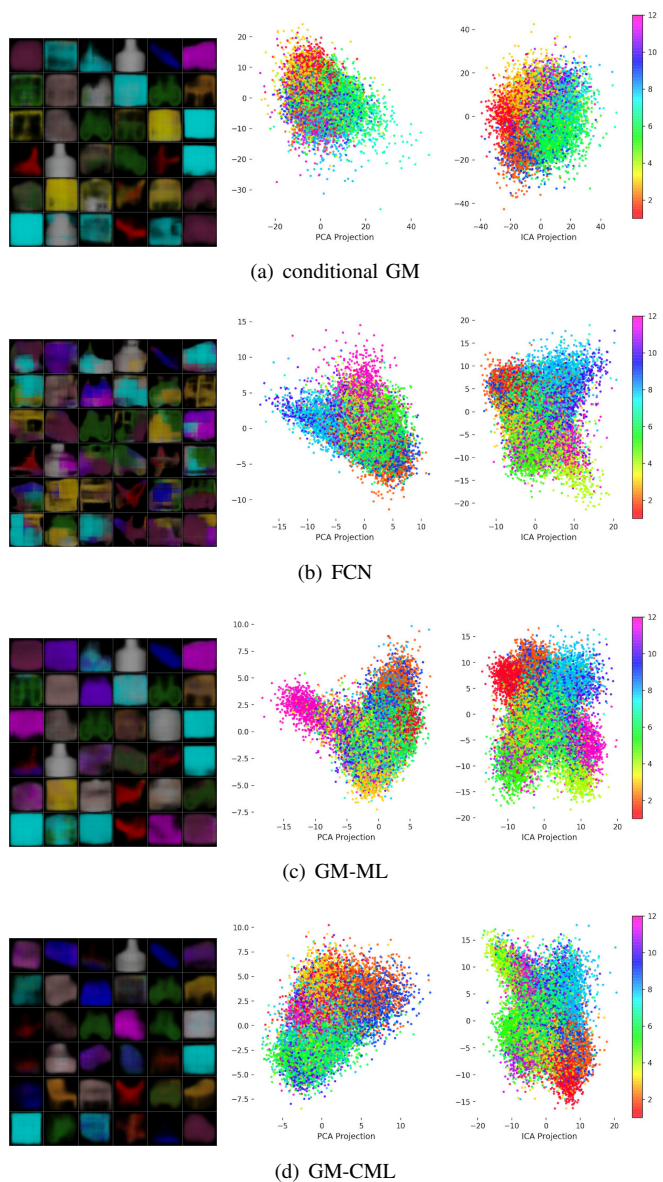


Fig. 12. Reconstruction samples of real images from ImageNet and low dimensional projection using PCA and ICA. GM-CML means that the conjugate generative model is trained with adaptive noises.

be stored on disk occupying about 20.2 MB including both reconstruction network and classification network and achieves highest accuracy compared to both SqueezeNet [36] and AlexNet.

### C. Experiments on Pascal 12 Database

We further test our generative model on a difficult test set provided by PASCAL 3D+ database. Test images selected from PASCAL 2012 [5] are much more complicated than ones from ImageNet where foreground objects are not centered and shot as a whole part. This means that parts of object without complete contour are captured in sample photos. Basic result is carried out on texture-less models provided in PASCAL 3D+ database which shows that a severe data migration problem makes it too hard to get a good performance no matter which network we choose where all accuracies are not higher than

TABLE II

CLASSIFICATION ON IMAGENET SAMPLES ATTACHED IN PASCAL 3D+ DATABASE. TRAINING DATA INCLUDES REAL PHOTOS, MODELS FROM PASCAL 3D+(PASMODEL) AND MODELS FROM SHAPENET(SHAMODEL). GM-CML<sub>1</sub> MEANS THAT OUR CONJUGATE GENERATIVE MODEL IS TRAINED WITH ADAPTIVE NOISES AND THE OUTPUT OF RECONSTRUCTION NETWORK IS CONCATENATED WITH THE INPUT OF ZIGZAGNET. GM-ML<sub>2</sub> MEANS THAT THE CLASSIFICATION NETWORK IS ALEXNET.

Method \ Data	Real photo	PASCAL 3D	ShapeNet
GM-CML <sub>1</sub>	-	27.8%	50.5%
GM-ML <sub>1</sub>	-	26.1%	49.2%
GM-ML <sub>2</sub>	-	25.1%	48.2%
FCN [18]	-	23.9%	38.4%
DeconvNet [20]	-	26.2%	40.2%
SR [14]	-	25.1%	40.1%
AlexNet [1]	55.8%	24%	39.6%
SqueezeNet [36]	45.5%	21.4%	35%
ZigzagNet [37]	55.9%	25.1%	42.7%
Inception V1 [2]	59%	21.9%	29.9%
Inception V4 [26]	-	23.7%	37.2%
ResidualNet [3]	-	19.1%	28.5%
LDO [8]	-	14.8%	25.5%

20% in Table.III. It's so necessary to use synthetic images rendered from textured model provided in ShapeNet database instead of ones from texture-less models in PASCAL 3D+ in such condition with incomplete foreground objects waiting to be recognized. Parametric network trained from ShapeNet models has 10% improvement on accuracy with the help of reconstructed foreground objects. As objects are not centered in test photos, three reconstructed channels help to reconstruct foreground objects and improve recognition accuracy to 29.7% which is already much higher than that from deep models like Inception V4 [26] which is only 20.1%. This phenomenon means that deep residual structures like ResidualNet [3] and Inception V4 [26] with strong fitting capability still have their weakness when training on synthetic data and testing on real photos with data migration problem without the help of pose information. The reason why direct classification networks like AlexNet without reconstruction sub-network fail to achieve acceptable accuracy as our model in complex condition is that our coordinate generative is assisted with metric learning targeting on utilizing common knowledge rather than over-fitting all information. This means that our generative model has its own limitation on fitting with input data, but the whole parametric model is tuned on fundamental knowledge like relative pose information which could be easily collected from synthetic data. As show in Table.III, the most amazing point is that the accuracy of our pipeline is nearly twice as high as ones trained without generative model which are 15.2% for FCN [18] concatenated with a classification network and 15.1% for DeconvNet [20]. Obvious advantage in classification against traditional pixel-wise reconstruction methods could be explained by reconstruction results shown in Fig. 12 where our method avoids problem of tearing foreground objects up into several different objects in form of rendering it with different

colors in Fig. 12(b). Close accuracy between our generative model and ZigzagNet indicates that pose information helps to enhance the ability of perceiving ground truth relative information which avoid over-fitting for uncommon or random category information in test samples. Here we can draw conclusion that our generative model with coordinate metric learning could try best to reconstruct foreground objects in a global view rather than a pixel-wise view like FCN where the surface colors are always pure, so over-fitting problem is avoided by not reconstructing clear foreground object object channels.

TABLE III

CLASSIFICATION ON PASCAL 2012 SAMPLES ATTACHED IN PASCAL 3D+ DATABASE. TRAINING DATA INCLUDES REAL PHOTOS, MODELS FROM PASCAL 3D+(PASMODEL) AND MODELS FROM SHAPENET(SHAMODEL). GM-CML<sub>1</sub> MEANS THAT OUR CONJUGATE GENERATIVE MODEL IS TRAINED WITH ADAPTIVE NOISES AND THE OUTPUT OF RECONSTRUCTION NETWORK IS CONCATENATED WITH THE INPUT OF ZIGZAGNET. GM-ML<sub>2</sub> MEANS THAT THE CLASSIFICATION NETWORK IS ALEXNET.

Method \ Data	Real photo	PASCAL 3D	ShapeNet
GM-CML <sub>1</sub>	-	18.1%	29.7%
GM-ML <sub>1</sub>	-	18%	29.4%
GM-ML <sub>2</sub>	-	17.2%	28%
FCN [18]	-	13.4%	15.2%
DeconvNet [20]	-	12.1%	15.1%
SR [14]	-	13.3%	16.9%
AlexNet [1]	39.2%	15.2%	20.7%
SqueezeNet [36]	32.9%	14.8%	19.6%
ZigzagNet [37]	42.9%	16.7%	27.9%
Inception V1 [2]	42.3%	14.7%	17.3%
Inception V4 [26]	-	16.7%	20.1%
ResidualNet [3]	-	12.3%	16.2%
LDO [8]	-	11.2%	18.7%

## VII. CONCLUSION

We designed a unified deep generative model with two concatenated sub-networks to do foreground object reconstruction and category based classification at the same time. We try to solve the ultimate target of training deep parametric model barely on synthetic images rendered from 3D models and testing on real images taken with hardwares like camera. A coordinate training strategy based on variance ratio makes our conjugate network work as a whole part in the training stage which converges faster and benefit more from each others. Experiments in real photos from ImageNet database attached in ShapeNet database shows that our generative model with coordinate metric learning achieves the state of the art classification accuracy of 50.5% trained on rendered data.

## ACKNOWLEDGMENT

This work was partially sponsored by supported by the NSFC (National Natural Science Foundation of China) under Grant No. 61375031, No. 61573068, No. 61471048, and

No.61273217, the Fundamental Research Funds for the Central Universities under Grant No. 2014ZD03-01, This work was also supported by Beijing Nova Program, CCF-Tencent Open Research Fund, and the Program for New Century Excellent Talents in University.

## REFERENCES

- [1] A. Krizhevsky, I. Sutskever, and G. E. Hinton, "Imagenet classification with deep convolutional neural networks," in *Advances in Neural Information Processing Systems* 25. Curran Associates, Inc., 2012, pp. 1097–1105.
- [2] C. Szegedy, W. Liu, Y. Jia, P. Sermanet, S. Reed, D. Anguelov, D. Erhan, V. Vanhoucke, and A. Rabinovich, "Going deeper with convolutions," *CoRR*, vol. abs/1409.4842, 2014. [Online]. Available: <http://arxiv.org/abs/1409.4842>
- [3] K. He, X. Zhang, S. Ren, and J. Sun, "Deep residual learning for image recognition," pp. 770–778, 2015.
- [4] O. Russakovsky, J. Deng, H. Su, J. Krause, S. Satheesh, S. Ma, Z. Huang, A. Karpathy, A. Khosla, M. S. Bernstein, A. C. Berg, and F. Li, "Imagenet large scale visual recognition challenge," *CoRR*, vol. abs/1409.0575, 2014. [Online]. Available: <http://arxiv.org/abs/1409.0575>
- [5] M. Everingham, S. M. Eslami, L. Van Gool, C. K. I. Williams, J. Winn, and A. Zisserman, "The pascal visual object classes challenge: A retrospective," *International Journal of Computer Vision*, vol. 111, no. 1, pp. 98–136, 2015.
- [6] M. Aubry, D. Maturana, A. Efros, B. Russell, and J. Sivic, "Seeing 3d chairs: exemplar part-based 2d-3d alignment using a large dataset of cad models," in *CVPR*, 2014.
- [7] X. Peng, B. Sun, K. Ali, and K. Saenko, "Exploring invariances in deep convolutional neural networks using synthetic images," *CoRR*, vol. abs/1412.7122, 2014. [Online]. Available: <http://arxiv.org/abs/1412.7122>
- [8] P. Wohlhart and V. Lepetit, "Learning descriptors for object recognition and 3d pose estimation," in *Proc. IEEE CVPR*, 2015.
- [9] H. Su, C. R. Qi, Y. Li, and L. J. Guibas, "Render for CNN: viewpoint estimation in images using cnns trained with rendered 3d model views," *CoRR*, vol. abs/1505.05641, 2015. [Online]. Available: <http://arxiv.org/abs/1505.05641>
- [10] J. Yim, H. Jung, B. I. Yoo, and C. Choi, "Rotating your face using multi-task deep neural network," in *2015 IEEE Conference on Computer Vision and Pattern Recognition (CVPR)*, 2015, pp. 676–684.
- [11] J. Yang, S. E. Reed, M.-H. Yang, and H. Lee, "Weakly-supervised disentangling with recurrent transformations for 3d view synthesis," in *Advances in Neural Information Processing Systems* 28, C. Cortes, N. Lawrence, D. Lee, M. Sugiyama, and R. Garnett, Eds. Curran Associates, Inc., 2015, pp. 1099–1107.
- [12] B. Pepik, R. Benenson, T. Ritschel, and B. Schiele, "What is holding back convnets for detection?" *CoRR*, vol. abs/1508.02844, 2015. [Online]. Available: <http://arxiv.org/abs/1508.02844>
- [13] R. Zhao, W. Ouyang, H. Li, and X. Wang, "Saliency detection by multi-context deep learning," in *2015 IEEE Conference on Computer Vision and Pattern Recognition (CVPR)*, 2015, pp. 1265–1274.
- [14] Y. Wang and W. Deng, "Self-restraint object recognition by model based cnn learning," in *2016 IEEE International Conference on Image Processing (ICIP)*, Sept 2016, pp. 654–658.
- [15] A. X. Chang, T. Funkhouser, L. Guibas, P. Hanrahan, Q. Huang, Z. Li, S. Savarese, M. Savva, S. Song, H. Su, J. Xiao, L. Yi, and F. Yu, "ShapeNet: An Information-Rich 3D Model Repository," Stanford University — Princeton University — Toyota Technological Institute at Chicago, Tech. Rep. arXiv:1512.03012 [cs.GR], 2015.
- [16] S. Gupta, P. A. Arbeláez, R. B. Girshick, and J. Malik, "Inferring 3d object pose in RGB-D images," *CoRR*, vol. abs/1502.04652, 2015. [Online]. Available: <http://arxiv.org/abs/1502.04652>
- [17] Y. Xiang, R. Mottaghi, and S. Savarese, "Beyond pascal: A benchmark for 3d object detection in the wild," in *IEEE WACV*, 2014.
- [18] J. Long, E. Shelhamer, and T. Darrell, "Fully convolutional networks for semantic segmentation," in *IEEE Conference on Computer Vision and Pattern Recognition*, 2015, pp. 3431–3440.
- [19] L. Wang, W. Ouyang, X. Wang, and H. Lu, "Visual tracking with fully convolutional networks," in *IEEE International Conference on Computer Vision*, 2015, pp. 3119–3127.
- [20] H. Noh, S. Hong, and B. Han, "Learning deconvolution network for semantic segmentation," pp. 1520–1528, 2015.
- [21] D. P. Kingma and M. Welling, "Auto-encoding variational bayes," 2013.
- [22] D. M. Blei, A. Kucukelbir, and J. D. Mcalliffe, "Variational inference: A review for statisticians," 2016.
- [23] K. Sohn, H. Lee, and X. Yan, "Learning structured output representation using deep conditional generative models," in *Advances in Neural Information Processing Systems* 28, C. Cortes, N. D. Lawrence, D. D. Lee, M. Sugiyama, and R. Garnett, Eds. Curran Associates, Inc., 2015, pp. 3483–3491.



- [24] D. P. Kingma, D. J. Rezende, S. Mohamed, and M. Welling, "Semi-supervised learning with deep generative models," *Advances in Neural Information Processing Systems*, vol. 4, pp. 3581–3589, 2014.
- [25] S. Hinterstoisser, S. Benhimane, V. Lepetit, P. Fua, and N. Navab, "Simultaneous recognition and homography extraction of local patches with a simple linear classifier," in *Proceedings of the BMVC*. BMVA Press, 2008, pp. 10.1–10.10.
- [26] C. Szegedy, S. Ioffe, and V. Vanhoucke, "Inception-v4, inception-resnet and the impact of residual connections on learning," *CoRR*, vol. abs/1602.07261, 2016. [Online]. Available: <http://arxiv.org/abs/1602.07261>
- [27] F. N. Iandola, M. W. Moskewicz, K. Ashraf, S. Han, W. J. Dally, and K. Keutzer, "Squeezenet: Alexnet-level accuracy with 50x fewer parameters and <1mb model size," *CoRR*, vol. abs/1602.07360, 2016. [Online]. Available: <http://arxiv.org/abs/1602.07360>
- [28] I. T. Jolliffe, "Principal component analysis," *Technometrics*, 2014.
- [29] J. Wang, Y. Song, T. Leung, C. Rosenberg, J. Wang, J. Philbin, B. Chen, and Y. Wu, "Learning fine-grained image similarity with deep ranking," *CoRR*, vol. abs/1404.4661, 2014. [Online]. Available: <http://arxiv.org/abs/1404.4661>
- [30] I. Goodfellow, J. Pouget-Abadie, M. Mirza, B. Xu, D. Warde-Farley, S. Ozair, A. Courville, and Y. Bengio, "Generative adversarial nets," in *Advances in Neural Information Processing Systems 27*, Z. Ghahramani, M. Welling, C. Cortes, N. D. Lawrence, and K. Q. Weinberger, Eds. Curran Associates, Inc., 2014, pp. 2672–2680.
- [31] A. Radford, L. Metz, and S. Chintala, "Unsupervised representation learning with deep convolutional generative adversarial networks," *CoRR*, vol. abs/1511.06434, 2015. [Online]. Available: <http://arxiv.org/abs/1511.06434>
- [32] A. Makhzani, J. Shlens, N. Jaitly, I. Goodfellow, and B. Frey, "Adversarial autoencoders," *arXiv preprint arXiv:1511.05644*, 2015.
- [33] D. K. Taleshmekaeil, A. Safari, and Y. Kong, "Using one hot residue number system(ohrns) for digital image processing," in *The 16th CSI International Symposium on Artificial Intelligence and Signal Processing (AISP 2012)*, May 2012, pp. 064–067.
- [34] I. T. Jolliffe, "Principal component analysis," *Springer Berlin*, vol. 87, no. 100, pp. 41–64, 1986.
- [35] H. Abdi and L. J. Williams, "Principal component analysis," *Wiley Interdisciplinary Reviews Computational Statistics*, vol. 2, no. 4, pp. 433–459, 2010.
- [36] F. N. Iandola, M. W. Moskewicz, K. Ashraf, S. Han, W. J. Dally, and K. Keutzer, "Squeezenet: Alexnet-level accuracy with 50x fewer parameters and <1mb model size," *CoRR*, vol. abs/1602.07360, 2016. [Online]. Available: <http://arxiv.org/abs/1602.07360>
- [37] Y. Wang, C. Cui, X. Zhou, and W. Deng, "Zigzagnet: Efficient deep learning for real object recognition based on 3d models," in *Asian Conference on Computer Vision (ACCV)*, Nov 2016.

**Yida Wang** received B.E. and M.E. degrees from Beijing University of Posts and Telecommunications (BUPT), Beijing, China in 2014 and 2017, respectively. His research interests include pattern recognition and computer vision. He has published several technical papers in international conferences with some oral presentations. He has two successful open source projects on synthetic data utilization and machine learning sponsored by Google Summer of Codes. He was invited by Microsoft Research for attending Microsoft Faculty Summit in 2016 for project of "CNTK on Mac: 2D Object Restoration and Recognition Based on 3D Model" which was awarded the second prize for Microsoft Open Source Challenge. He was named of Excellent Graduate Student of Beijing City twice in 2014 and 2017, respectively.

**Weihong Deng** received the B.E. degree in information engineering and the Ph.D. degree in signal and information processing from the Beijing University of Posts and Telecommunications (BUPT), Beijing, China, in 2004 and 2009, respectively. From Oct. 2007 to Dec. 2008, he was a postgraduate exchange student in the School of Information Technologies, University of Sydney, Australia, under the support of the China Scholarship Council. He is currently an associate professor in School of Information and Telecommunications Engineering, BUPT. His research interests include statistical pattern recognition and computer vision, with a particular emphasis in face recognition. He has published over 30 technical papers in international journals and conferences, including a technical comment on face recognition in SCIENCE magazine. He also serves as the reviewer for several international journals, such as IEEE TPAMI, IJCV, IEEE TIP, IEEE TIFS, PR, and IEEE TSMC-B. His Dissertation titled Highly accurate face recognition algorithms was awarded the Outstanding Doctoral Dissertation by Beijing Municipal Commission of Education in 2011. He was named New Century Excellent Talents by the Ministry of Education of China in 2013.